JMEPEG (2009) 18:588–593
DOI: 10.1007/s11665-009-9428-4

1059-9495/$19.00

Development of Texture and Microstructure During Cold Rolling and Annealing of a Fe-Based Shape Memory Alloy

Bikas C. Maji, Madangopal Krishnan, Vijay Hiwarkar, Indradev Samajdar, and R.K. Ray

(Submitted October 13, 2008; in revised form February 21, 2009)

Texture evolution and microstructural changes during cold rolling and annealing of Fe-14Mn-6Si-9Cr-5Ni shape memory alloy have been investigated. The starting solution-annealed material has a nearly random texture with microstructure composed of equiaxed austenite grains with ε martensite plates inside. Cold rolling induces a strong alloy type texture with Brass {011}⟨211⟩ and Goss {011}⟨100⟩ as major components. Annealing of the cold-deformed material produces a nearly random texture. The microstructural investigation reveals that with increase in cold deformation, the amount of stress-induced ε and α′ martensite volumes increase. The electron back-scattered diffraction (EBSD) phase mapping shows that reversion of the ε martensite begins only after recrystallization sets in at a temperature of 1073 K.

Keywords EBSD, shape memory alloy, texture

1. Introduction

The Fe-Mn-Si-based shape memory alloys have been extensively investigated for the past few decades due to their potential application as low-cost shape memory alloys. The shape memory effect (SME) in these alloys owes its origin to the γ to ε martensitic transformation. The SME in these alloys was first discovered by Sato et al. (Ref 1) who investigated single-crystal Fe-30Mn-1Si alloy in early 1980s. They showed that the SME in these material is strongly dependent on the crystallographic orientation in such a way that up to 8% tensile strain, a nearly perfect recovery (100%) could be obtained along the ⟨441⟩ direction. By contrast, a remarkably suppressed recovery (∼15%) was noticed along the ⟨100⟩ direction. The SME observed in polycrystalline Fe-Mn-Si-based shape memory alloys, developed so far, is also limited to a maximum 3% recoverable strain only, which is much smaller than what has been reported for the single crystal. Therefore, introducing proper texture in the parent phase during processing could be an effective approach for improving the SME of these alloys. However, so far no systematic study on development of texture and microstructure during cold deformation and annealing of Fe-based shape memory alloys has been reported in published literature. In the present work, an attempt has been made to study the development of texture and microstructure during cold rolling and annealing in Fe-14Mn-6Si-9Cr-5Ni shape memory alloy.

This article is an invited paper selected from presentations at Shape Memory and Superelastic Technologies 2008, held September 21-25, 2008, in Stresa, Italy, and has been expanded from the original presentation.

Bikas C. Maji and **Madangopal Krishnan**, Materials Science Division, Bhabha Atomic Research Centre, Mumbai 400 085, India; **Vijay Hiwarkar** and **Indradev Samajdar**, Department of Metallurgical Engineering and Materials Science, Indian Institute of Technology, Powai, Mumbai 400 076, India; and **R.K. Ray**, R&D Division, Tata Steel, Jamshedpur 831 001, India. Contact e-mail: madangk@barc.gov.in.

2. Experimental

The Fe-14Mn-6Si-9Cr-5Ni (in mass%) alloy used in this study was prepared by nonconsumable vacuum arc melting using high purity Fe, Mn, Si, Cr, and Ni. The arc-melted button was hot rolled at 1173 K into a strip of 2 mm thickness. This strip was solution annealed at 1323 K for 1 h and further cold rolled at room temperature to 6, 20, 35, and 45% reduction in thickness. Annealing study was carried out in the temperature range of 873-1373 K using the maximum deformed (45% reduction in thickness) specimen. The forward and reverse martensitic transformation temperatures for this alloy as measured by differential scanning calorimeter (DSC) after solution annealing treatment are found to be M_s = 291 K, M_f = 257 K, A_s = 393 K, and A_f = 413 K. The microstructural evolution was characterized using an optical microscope, x-ray diffractometer, and a FEI Quanta 200 HV tungsten filament scanning electron microscope (SEM) equipped with TSL (TexSEM Laboratories, Incorporated) orientation imaging microscopy (OIM) system. The x-ray diffractometry (XRD) and bulk texture measurement were carried out using MoK_α (λ = 0.7093 Å) x-radiation in rectangular specimens of 20 mm × 15 mm size which were mechanically ground and polished up to the mid thicknesses level. The XRD measurements were carried out in 2θ range of 15°-55° and at a scanning speed 0.6°/min. Both pole figure and orientation distribution function (ODF) methods were employed to study the texture development in the parent austenite phase. The optical microstructures of these specimens were revealed by electroetching,

using a solution of $CH_3OH + HCl$ (90:10 volume ratio) and 6 V dc potential supply. The electron back scatter diffraction (EBSD) measurements were conducted at 20 kV with a step size between 0.5 and 0.2 μm in an area about 400 μm × 400 μm.

3. Results

3.1 Microstructure and Texture of the Starting Material

Figure 1(a) shows the optical micrograph of the starting material which was prepared by solution annealing of the hot-rolled material at 1323 K for 1 h followed by water quenching. The microstructure reveals equiaxed austenite grains (~70 μm in size) with some parallel lines inside. These lines are mostly ε martensite plates which must have been formed during water quenching of the specimen. Apart from these, some annealing twins with straight boundaries are also observed within the microstructure. The {111} pole figure of the austenite phase is shown in Fig. 1(b). The pole figure indicates that the material has a nearly random texture, with some isolated weak peaks.

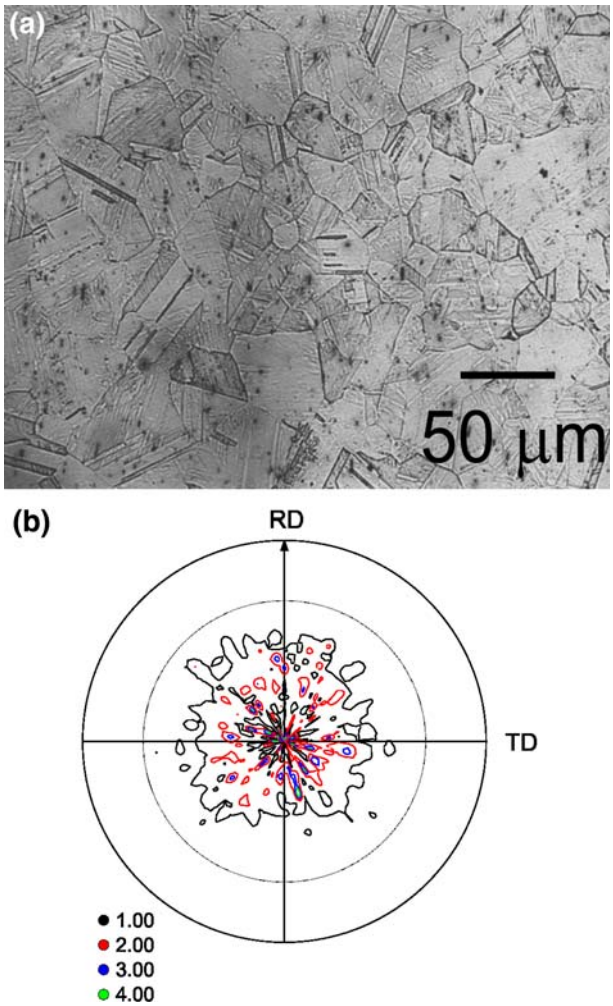

Fig. 1 (a) Optical micrograph and (b) the {111} austenite pole figure of the starting material solution annealed at 1323 K for 1 h

3.2 Microstructural Changes During Cold Rolling

Figure 2 displays the XRD patterns obtained from the mid-thickness levels of the specimens at different stages of cold-rolling reduction. In this figure, the gradual changes in phase constitutions during the progress of cold rolling are compared with that of the starting solution-annealed specimen. After 6% cold rolling (Fig. 2b), mainly, the austenite and ε martensite phase which form due to stress-induced transformation of the parent austenite are present. However, after 20% cold rolling, formation of α′ martensite can be clearly identified by the presence of distinct XRD peaks. The α′ martensite possibly forms due to the interaction of different ε martensite variants during cold deformation (Ref 2, 3). Another interesting observation is that the (002) peak of the parent austenite phase disappears after 20% cold rolling, indicating that the material is getting textured. The intensities of the α′ martensite peaks increase with further increase in cold reduction. At higher amount of strain (more than 20%), peak broadening has been noticed which is possibly associated with accommodation of heavy strain that leads to fragmentation of grains (Ref 4, 5). Some of the peaks could be due to the merging of peaks arising from the two different types of martensite phases.

Optical microscopy of longitudinal sections of the cold-rolled specimens was done. Figure 3(a) shows the microstructure of a specimen cold rolled to 6%. It can be seen that a large amount of ε martensite plates have formed within the austenite grains, and in some places, the fragmentation of grains due to localized deformation has begun. The microstructure after 20% cold rolling becomes highly inhomogeneous, and austenite grains get further fragmented. Beyond 35% reduction in thickness, shear bands and deformation bands are observed to occur. Figure 3(b), taken from a specimen after 45% cold rolling, clearly shows that austenite grains become highly elongated along the rolling direction and extremely thin in the thickness direction. A large number of deformation bands can also be noticed.

3.3 Texture Development During Cold Rolling

Texture development has been investigated by measuring three incomplete pole figures, {111}, {110}, and {311}, using

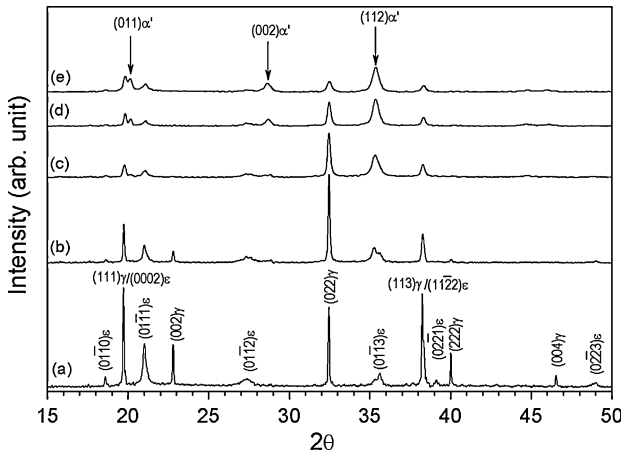

Fig. 2 XRD patterns obtained from specimens after (a) solution annealing, (b) 6%, (c) 20%, (d) 35%, and (e) 45% cold-rolling reductions shows the gradual change in phase constituents

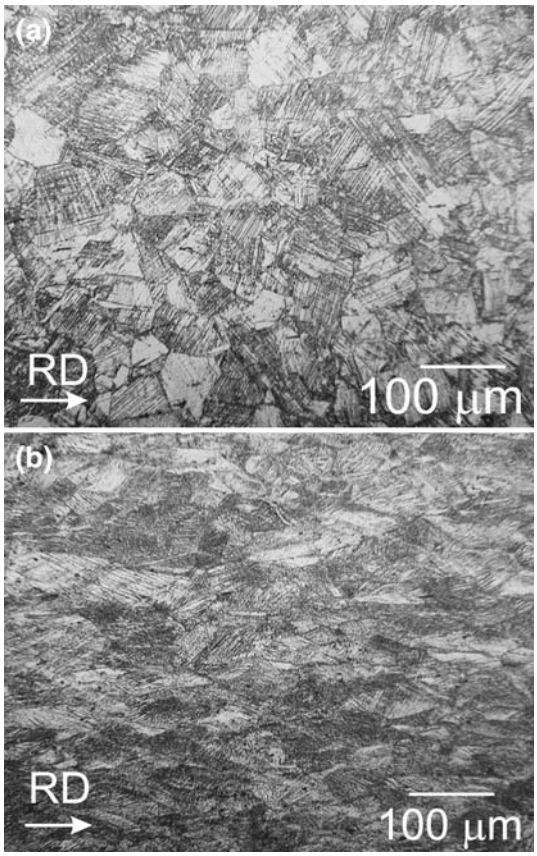

Fig. 3 Optical micrographs of the longitudinal sections after (a) 6% and (b) 45% reduction in thickness. Formation of shear band and deformation bands are noticed after 45% cold rolling

the Schultz (Ref 6) reflection technique. Three-dimensional ODFs were calculated on the basis of Bunge's series expansion method (Ref 7). Figure 4(a) shows the measured {111} pole figure obtained from specimens cold rolled by 20%. It can be seen that the spread of intensities is close to the $\{110\}\langle 112\rangle$ Brass orientation. Further reduction in thickness is seen to lead to sharpening of the texture intensity. However, no other orientations appear in the pole figure till 45% reduction. An orientation is most adequately represented as a point in three-dimensional orientation space, for instance, by the three Eulerian angles, ϕ_1, ϕ, and ϕ_2, in the reduced Eulerian space. Traditionally, the ODF is represented in sections of ϕ_2 = const. for fcc materials. The $\phi_2 = 0°$, 45°, and 65° sections of the ODFs of the fcc materials are very useful for showing the typical texture components that are present. Figure 4(b) shows these ODF sections of the 45% cold-rolled specimens. Presence of a strong Brass component $\{110\}\langle 112\rangle$ at $\phi_1 = 35°$, $\phi = 45°$ in the $\phi_2 = 0°$ section and $\phi_1 = 55°$, $\phi = 90°$ in the $\phi_2 = 45°$ section can be seen in this figure. Apart from the Brass orientation, the presence of Copper orientation $\{112\}\langle 111\rangle$ is also observed at $\phi_1 = 90°$, $\phi = 35°$ in the $\phi_2 = 45°$ section. At $\phi_1 = 60°$, $\phi = 35°$ in the $\phi_2 = 65°$ section, another texture component with a broad intensity spread is noticed. This could be the $\{123\}\langle 634\rangle$ S orientation which normally appears in between Brass and Copper orientations. In addition to the ODF sections, the orientation density along certain fibers in Euler space contain the most important texture components and give a good overview of the rolling texture development. For fcc phase a clear view of the texture development can be obtained by plotting the ODF intensity along the α and β-fibers. Figure 5 shows the intensity change in (a) α-fiber and (b) β-fiber with deformation obtained from specimens cold rolled to 20% and 45% reduction, respectively. The major texture components in

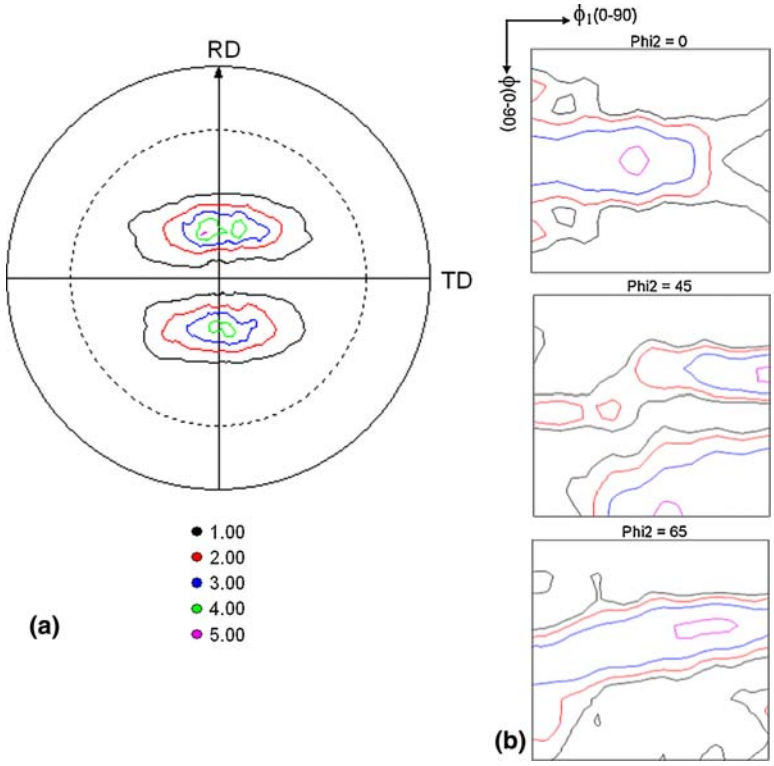

Fig. 4 (a) The {111} pole figure of the 20% cold-rolled specimen and (b) the ODFs sections of the 45% cold-rolled material

the α-fiber is Brass, with which a minor Goss {110}⟨001⟩ is also observed. It is seen that while Brass orientation markedly intensifies with increasing reduction, Goss orientation remains at a relatively low intensity. The β-fiber plots, Fig. 5(b), for 20% and 45% reductions are remarkably uniform, though the overall texture intensity of the fiber tends to increase with increasing rolling reduction.

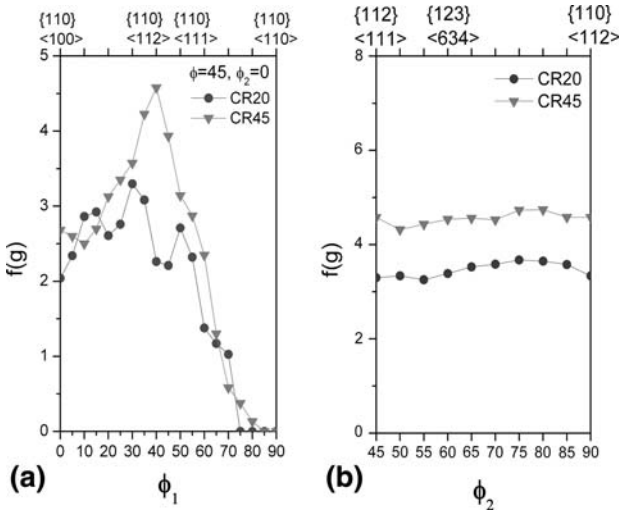

Fig. 5 The variation of texture intensity along (a) the α-fiber and (b) the β-fiber with increasing cold deformation

3.4 Textural and Microstructural Changes During Annealing

The development of texture during annealing was measured after isochronal annealing treatments of 1 h at 973, 1123, 1173, and 1273 K. Figure 6 shows a gradual change in the {111} pole figures with increasing annealing temperature. The figure also indicates that noticeable change occurs only above annealing temperature of 1123 K (Fig. 6b). Further increase in annealing temperature only leads to spreading of texture intensity (Fig. 6c). The overall texture intensity shows a gradual decrease with increase in annealing temperature and annealing at 1273 K (Fig. 6d) results in a nearly random texture.

Figure 7 displays a few optical micrographs of the annealed specimens. Figure 7(a) shows that cold-worked structure persists till 973 K. The recrystallization process starts at 1123 K, as evidenced in Fig. 7(b). However, in this microstructure some cold-worked areas are still observed. Annealing at 1173 K (Fig. 7c) is observed to give rise to a completely recrystallized microstructure.

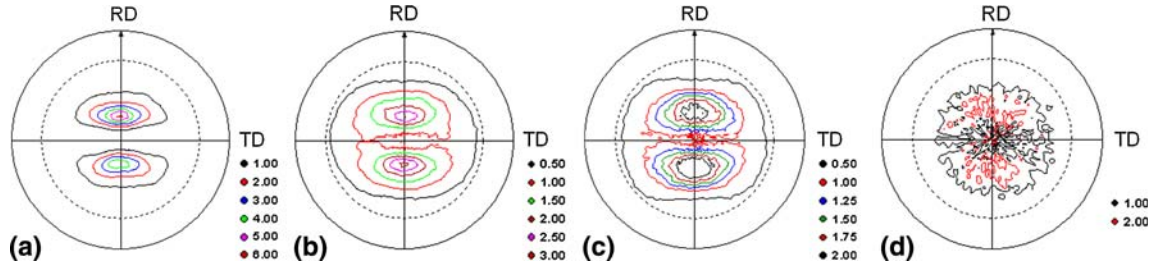

Fig. 6 The {111} pole figures obtained from specimens after 1 h isochronal annealing at (a) 973 K, (b) 1123 K, (c) 1173 K, and (d) 1273 K

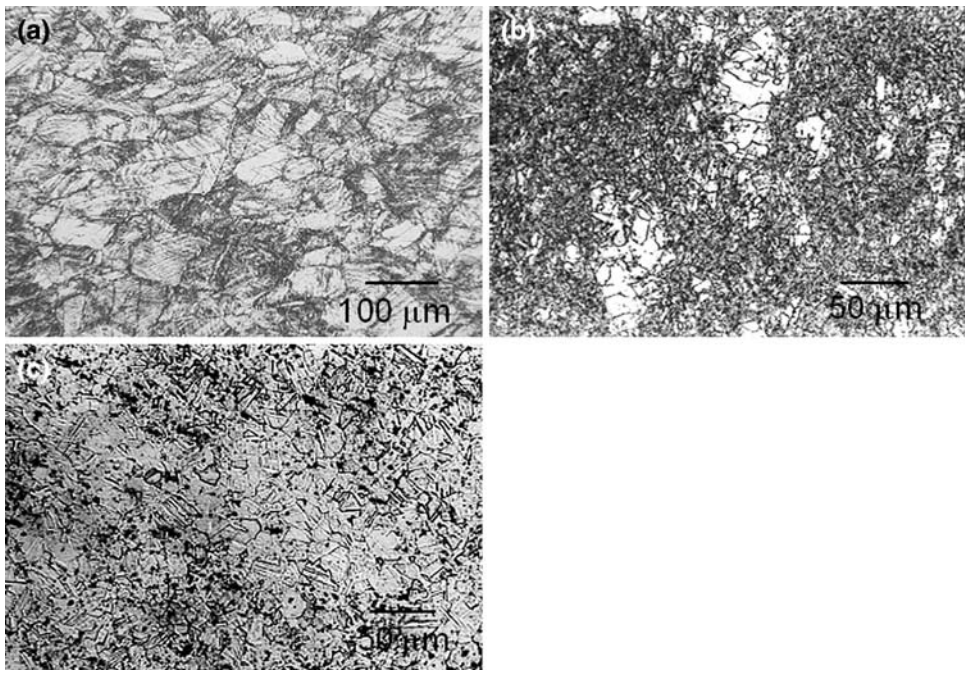

Fig. 7 The optical micrographs of specimens annealed at (a) 973 K, (b) 1123 K, and (c) 1173 K for 1 h

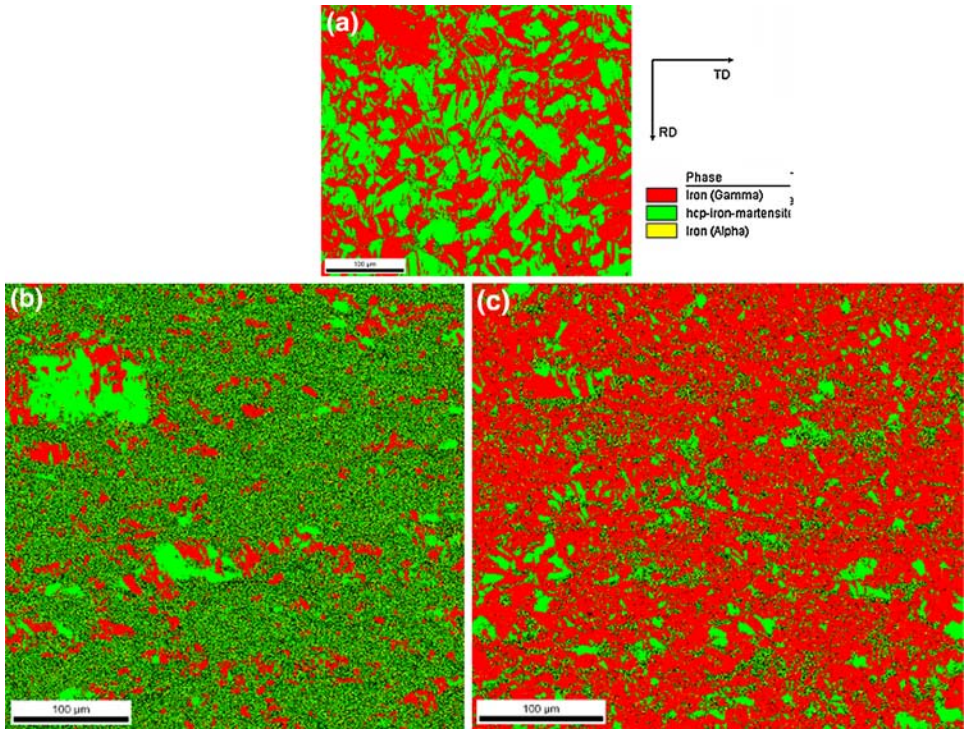

Fig. 8 EBSD phase maps of specimens after (a) 6% cold rolling, (b) annealing at 973 K for 1 h, and (c) annealing at 1123 K for 1 h

3.5 EBSD Phase Mapping

The EBSD phase maps were obtained at each stage of cold reduction. Figure 8(a) shows a typical map obtained from a specimen cold deformed by 6%. The map essentially reveals that at lower deformation levels, austenite phase transforms to ε martensite. However, fragmentation of grains starts beyond 20% cold deformation. The relative changes in volume fractions of different constituent phases with increased cold reduction, as measured by the EBSD phase mapping, are given in Table 1.

EBSD phase maps obtained after isochronal annealing show interesting results. For example, after 1 h isochronal annealing of the 45% deformed sample at 973 K (Fig. 8b) does not show much of austenite phase. On the other hand, for the specimen annealed at 1123 K that was initially deformed to similar extent (Fig. 8c) clearly shows a large volume fraction of austenite. It is also observed that the 1123 K annealed specimen is mostly recrystallized, whereas recrystallization has not initiated in the 973 K one. This suggests that austenite reversion takes place only after recrystallization starts.

Table 1 Relative change in volume fraction of constituent phases with cold rolling

Cold rolling amount (% reduction in thickness)	Austenite (vol. fraction)	ε martensite (vol. fraction)	α′ martensite (vol. fraction)
6	0.55	0.44	0.01
20	0.22	0.64	0.14
35	0.11	0.72	0.17
45	0.07	0.75	0.18

4. Discussion

The cold-rolling texture of this material is quite typical of low stacking fault energy fcc alloys that are cold deformed by moderate (<50%) extents. It was observed that this material could be cold rolled only up to 45%, before cracks could begin appearing. It is possible that the large amount of Mn and Si present in this alloy cause a high rate of work hardening. The room temperature stacking fault energy was calculated using Eq 1 of Ref 8 and found to be ~3.41 mJ/m^2. The cold-rolling texture of heavily deformed (~95%) fcc material of comparable stacking fault energy usually shows a large volume fraction of the Brass {110}⟨112⟩ component. This has been seen in a 95% cold-rolled Ni-60Co alloy with stacking fault energy of ~13 mJ/m^2 (Ref 9). However, after 40% cold rolling, the same alloy shows a rather uniform β-fiber (Ref 10)—the type that has been observed in this study after 45% cold reduction. Thus, it can be said that the texture evolution in this alloy during cold rolling is similar to that of fcc materials with low SFE.

Annealing of the 45% cold-rolled material shows a gradual change in the texture evolution. The overall texture intensity decreases with increase in annealing temperature, although, the basic nature of the texture does not change. After the material is fully recrystallized, above annealing temperatures of 1173 K, texture intensity decreases drastically, although, the main Brass component of texture persists. This clearly indicates a nucleation-dominated recrystallization process. The inverse pole figure (Fig. 9) taken from the recrystallized sample substantiates this point. Recrystallization at higher temperatures leads to grain growth. In fact, the average grain size after 1273 K annealing is 6 to 7 times that after 1173 K annealing (fully recrystallized). The pole figure correspondingly shows a random distribution of discrete spots. It is interesting to note

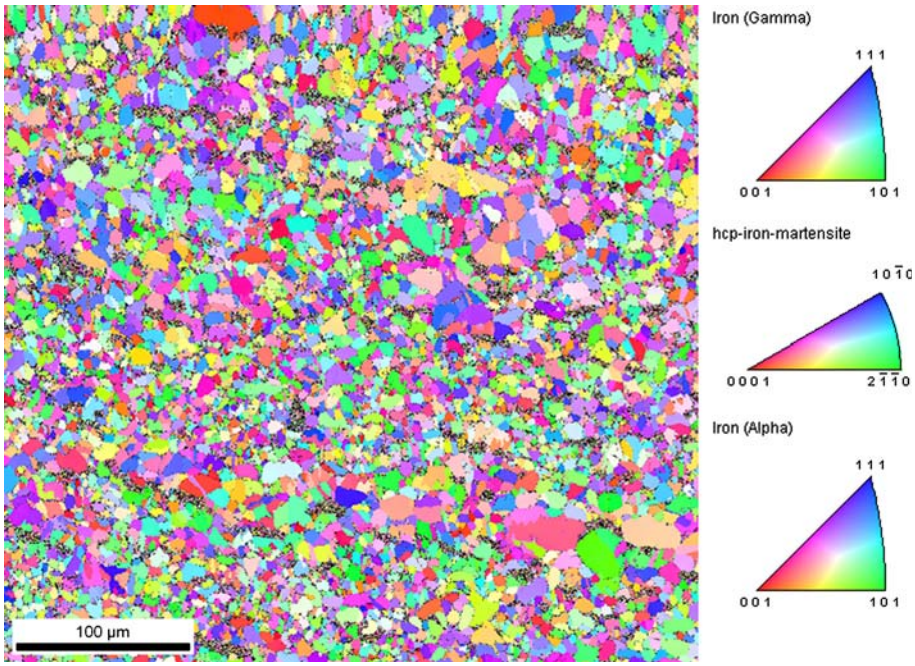

Fig. 9 Inverse pole figure map of the fully recrystallized specimen (annealed at 1173 K for 1 h) shows that the orientations of freshly nucleated recrystallized grains are random

that the overall texture intensity does not show any change during grain coarsening.

The textural changes in this alloy are accompanied by the γ-ε-α′ martensitic phase transformation. The parent austenite transforms to hcp ε martensite, which further transforms to bcc α′ martensite through the interaction of different ε variants (Ref 2, 3). The observation, that the reverse transformation occurs only after recrystallization begins, suggests that the driving force for the reverse transformation is high. In fact, the extent of reversion increases with progress of recrystallization. Further studies will be required to determine the precise reason for this behavior.

5. Summary

1. Cold deformation induces a strong alloy-type texture with Brass {110}⟨112⟩ as the major component.
2. Cold deformation above 6% results in formation of strain-induced α′ martensite.
3. Complete recrystallization of cold-deformed material results in random texture.
4. Reverse transformation of stress-induced ε martensite starts only after initiation of recrystallization.

References

1. A. Sato, E. Chishima, K. Soma, and T. Mori, Shape Memory Effect in γ-ε Transformation in Fe-30Mn-1Si Alloy Single Crystals, *Acta Metall.*, 1982, **30**(6), p 1177–1183
2. J.H. Yang and C.M. Wayman, Development of Fe-Based Shape Memory Alloys Associated with Face-Centered Cubic-Hexagonal Closed-Packed Martensitic Transformations: Part III. Microstructures, *Metall. Trans. A*, 1992, **23**(5), p 1445–1454
3. B.C. Maji and M. Krishnan, The Effect of Microstructure on the Shape Recovery of Fe-Mn-Si-Cr-Ni Stainless Steel Shape Memory Alloy, *Scr. Mater.*, 2003, **48**, p 71–77
4. B.D. Cullity, *Elements of X-ray Diffraction*, 2nd ed., Addison-Wesley, Reading, MA, 1978, p 285–292
5. B.L. Averbach and B.E. Warren, The Effect of Cold Work in Metals on Powder Pattern Intensities, *J. Appl. Phys.*, 1949, **20**, p 1066–1069
6. L.G. Schulz, A Direct Method of Determining Preferred Orientation of a Flat Reflection Sample Using a Geiger Counter X-ray Spectrometer, *J. Appl. Phys.*, 1949, **20**, p 1030–1033
7. H.J. Bunge, *Texture Analysis in Materials Science*, Butterworth, London, 1982
8. H. Li, F. Yin, T. Sawaguchi, K. Ogawa, X. Zhao, and K. Tsuzaki, Texture Evolution Analysis of Warm-Rolled Fe-28Mn-6Si-5Cr Shape Memory Alloy, *Mater. Sci. Eng. A*, 2008, **494**, p 217–226
9. R.K. Ray, Rolling Texture of Pure Nickel, Nickel-Iron and Nickel-Cobalt Alloys, *Acta Metall. Mater.*, 1995, **43**(10), p 3861–3872
10. R.K. Ray, R&D Division, Tata Steel, Personal communication, 2008